Hindawi
International Journal of Intelligent Systems
Volume 2023, Article ID 6664219, 13 pages
https://doi.org/10.1155/2023/6664219

Research Article

Smart City Facility Location Recommendation Algorithm Using Multimedia Data and Improved Generative Adversarial Networks

Xueqing Xie and Ming He

Institute of Design, Chongqing Industry Polytechnic College, Chongqing 401120, China

Correspondence should be addressed to Ming He; heming@cqipc.edu.cn

Received 20 February 2023; Revised 25 June 2023; Accepted 4 July 2023; Published 15 July 2023

Academic Editor: B. B. Gupta

Internet of Things, low energy consumption, and intelligent and functionally integrated urban infrastructure construction are crucial elements in the development of smart cities. Distributed generation (DG) and electric vehicle charging infrastructure play a vital role in the planning and construction of smart cities. However, the uncertainty associated with the power output of distributed generation significantly impacts the planning of distribution networks. To address this issue, this paper proposes a site-selection recommendation algorithm that leverages urban multimedia data and improved generative adversarial networks. The proposed algorithm begins by modeling the uncertainty of wind power and photovoltaic (PV) generation using an enhanced conditional generative adversarial network model. To generate multimedia datasets with time-series characteristics for wind power and PV generation scenarios, monthly multimedia data labels are incorporated into the model. These multimedia datasets, representing a wide range of scenarios, are then clustered using the *K*-means clustering method. Furthermore, a distributed generation planning model is established, aiming to minimize the annual integrated cost. The planning problem is efficiently solved using CPLEX, a mathematical programming solver. In the simulation experiments, the proposed scheme is compared with alternative schemes. The results demonstrate that the proposed scheme achieves a significant total cost saving of 21.95% compared to the comparison scheme. Moreover, the experimental comparison reveals that the proposed scheme exhibits higher stability. Additionally, in terms of algorithm efficiency, the proposed algorithm outperforms the other three algorithms tested in terms of the number of iterations and speed. The experimental results highlight the effectiveness of the proposed planning model in improving the economy and stability of the distribution network. Furthermore, it enhances the computational efficiency of the planning problem associated with distributed power supply and electric vehicle charging stations. The findings of this research hold substantial research significance for the site selection planning of distributed power supply.

1. Introduction

tWith the advancement of the Internet of Things, cloud computing, and multimedia technologies, the concept of "smart cities" has been gaining prominence as the future direction of urban planning and development. The goal of urban planning is to leverage big data and artificial intelligence to enhance the quality of life for the inhabitants and establish sustainable and people-centric cities. Facility siting has emerged as a significant concern in the context of smart cities and has found applications in diverse domains [1, 2]. In the 21st century, electric vehicles play a crucial role in realizing a low-carbon environment and establishing a robust smart grid [3]. For ease of understanding, each acronym and its corresponding full explanation are listed here, as shown in Table 1.

As an ideal substitute for fuel vehicles, EVs are rapidly emerging in the market with their advantages of low pollution, low emissions, and high energy utilization. In the near future, the ratio of traditional fuel vehicles to EVs will change significantly, and the reasonable planning of charging facilities is the key to further promoting the development of EVs [4]. As the proportion of EVs continues to increase, the randomness of their charging loads exacerbates the load-side uncertainty. EV charging loads have a certain degree of randomness in both time and space. In areas with

Table 1: List of abbreviations.

Abbreviations	Full explanation
IoT	Internet of Things
DG	Distributed generation
PV	Photovoltaic
EV	Electric vehicle
CPLEX	CPLEX mathematical programming solver
GAN	Generative adversarial network
WGAN	Wasserstein generative adversarial network
GP	Gradient penalty
CGAN	Conditional generative adversarial network
LAPGAN	Laplacian pyramid generative adversarial network
LSGAN	Least squares generative adversarial network
ACGAN	Auxiliary classifier generative adversarial network
BN	Batch normalization

dense electricity consumption loads, the charging behavior of EVs will increase the pressure of power supply in the power system. During peak hours, the access of EV charging load will further aggravate the peak-valley difference in load, which has a certain impact on the safe and reliable operation of the distribution network and electricity-using equipment. With the increase in EV users, it greatly complicates the structure of the distribution network and brings new impact and challenges to the location of DG.

In response to this situation, scholars at home and abroad have conducted relevant research on the siting of DG. Ufa et al. [5] established a mathematical model for the planning of DG with the main objective of economic cost and the total cost of annual construction investment, operation and maintenance, power purchase, and environmental protection. Liu et al. [6] introduced environmental coordination factors, thus adding the environmental and social benefits of DG and V2G into the optimization objective function, and built a constant volume model of DG location considering V2G. Veeresha et al. [7] used the K-means clustering algorithm to reduce the operating scenarios and obtained a typical operating scenario model with diversity. He et al. [8] considered the uncertainty of the output power of wind turbine and photovoltaic generators and expressed it by fuzzy variables; the objective function was to minimize the annual investment and operation cost, and the constraints of economic and reliable operations were used. Jiménez-Fernández et al. [9] took the maximum benefit of independent generators as the objective function and adopted the simulated plant growth algorithm to establish the location planning model of DG access to the distribution network. Venkatesan et al. [10] considered the uncertainty of DG output and built a planning model with a minimum energy cost. Panda et al. [11] designed a DG configuration model for EV impact and demand-side management based on the consideration of DG output volatility and then solved it by the differential evolutionary algorithm and the original pairwise interior point method. Shuaibu Hassan et al. [12] used the DG planning model, in which the environmental pollution cost generated by microgas turbines is taken into account and solved using a genetic algorithm. Jallad et al. [13] proposed an improved firefly algorithm for solving the DG planning model with the objective of minimizing the cost of economic loss due to voltage dips.

Although the abovementioned literature has made some progress in the problem of stochastic optimal allocation of DG capacity, most of the current generation scenarios use sampling methods such as Latin hypercube and Monte Carlo, which require prior assumptions that the data obey a specific probability distribution before using these sampling methods. A generative adversarial network (GAN), on the other hand, learns from multimedia data directly and generates new multimedia data samples without assuming that the data obey a specific probability distribution in advance [14]. Therefore, GAN has received a lot of attention since it was proposed.

Based on the aforementioned research, this paper addresses the issue of generating unrealistic scenarios caused by the disparity between assumed and actual multimedia data distributions in traditional sampling methods. To overcome this, an enhanced conditional generative adversarial network model is employed, which does not rely on prior assumptions about the original multimedia data distribution. This model is utilized to generate wind and photovoltaic (PV) output scenarios based on real multimedia data. Subsequently, a distributed generation (DG) optimization allocation model is formulated with the objective of minimizing the annual integrated cost. Through simulation experiments, the effectiveness of the proposed planning model is validated, providing valuable insights for the analysis of the EV charging load's spatiotemporal distribution and DG site selection.

2. State of the Art

2.1. Development of GAN. Generative adversarial networks have become a hot research topic in academia since their introduction, and many excellent researchers have improved and optimized them from different perspectives. The original GAN network only takes noise as input and cannot control the output of the network model [15]. Some scholars proposed a conditional generative adversarial network (CGAN) [16] based on GAN, which adds conditional information to the input of the original model structure so that the output of the model can be influenced by the specified input conditions. Some scholars proposed ACGAN [17] on the basis of CGAN, which adds category judgments while identifying the authenticity of images, allowing the network to better learn the data features of the samples and generate high-quality images. Other scholars proposed Triple-GAN [18], which adds classifiers to the structure of CGAN and uses classifiers and generators to simultaneously learn the multimedia data labels and the conditional distribution of images. It can generate more multimedia datasets while generating better images, reducing the cost of manual labeling.

The original GAN network uses a fully connected layer architecture, which can only generate images with low resolution due to the large number of parameters. Therefore, many researchers have improved and optimized the network

structure to generate higher quality images. Some scholars proposed the LAPGAN model [19]. It uses the cascaded generative adversarial network, takes the picture generated at the upper level as the condition variable of the next level, and then uses this Laplacian pyramid structure to generate the precise picture. Other scholars proposed StackGAN [20]. This approach generates low-resolution images in the first stage by using two successive generator models and generates high-resolution graphs in the second stage using the generated low-resolution images and text descriptions as conditional information inputs. This hierarchical model framework effectively improves the network's ability to generate high-resolution images.

The original GAN network also uses JS divergence to measure the disparity of data distribution, which is prone to the problem of training instability [21]. Therefore, many researchers have tried to use a better distance measure. Some scholars have proposed LSGAN [22]. This model uses a least squares loss function to replace the cross-entropy loss function of the original GAN network, which makes the training of the GAN network more stable and generates higher quality images. Other scholars proposed Wasserstein Generative Adversarial Network (WGAN) and Wasserstein distance and used them to construct the evaluation function [23]. This method solves the problem of gradient disappearance and instability caused by the JS divergence as the evaluation function and reduces the difficulty of network training. To address the problems of gradient disappearance and parameter centralization during training of WGAN, the team also proposed the Gradient Penalized Generative Adversarial Network-Gradient Penalty (WGAN-GP), which introduces a gradient penalty strategy to further improve and optimize WGAN.

GAN networks have been widely studied because of their powerful generative power. In addition to improving and optimizing GAN from the abovementioned perspectives, many studies have been conducted on improving the training techniques of GAN networks. Many researchers have improved and optimized GAN networks from different perspectives, and many researchers have summarized and concluded the development history of GAN networks. Some of the GAN network development genealogies mentioned in this paper are shown in Table 2.

2.2. Research on GAN in Urban Planning. Machine learning builds on traditional big data analysis methods to make decisions and predictions about urban construction by using input multimedia data and algorithms to estimate unknown outcomes. Among machine learning models, GAN is a deep learning architecture proposed by Newton [24] from the University of Montreal in 2019. It aims to model the distribution of the latter through the generated multimedia data sample information with natural images, enabling the GAN to learn and generate higher-order features. To build a predictive model for urban facility planning using GAN, multimedia datasets need to be produced to be fed into the generator and discriminator for training so that the generated images obtained from the input multimedia dataset in the generator are counterbalanced with the real images in the output multimedia dataset. Generative adversarial networks have become an important tool in the current study of urban space, and their predictive features can be used to generate urban images or interest point layouts. Zhao et al. [25] applied the WGAN-GP algorithm to generate topography and build masks to predict elevation information for unknown areas. Ji et al. [26] generated multimedia datasets to predict building rows in urban planning maps based on labeled spatial elements such as roads, green spaces, and rivers. Man et al. [27] used the Pix2PixHD algorithm to combine pedestrian flow and urban spatial multimedia data to predict heat maps of street hawker distribution. Newton et al. [24] used the pix2pix technique to conduct a morphogenetic simulation of residential areas. Li et al. [28] conducted a plan generation simulation of building clusters using the WGAN technique. Gong et al. [29] proposed the use of GAN to process unfamiliar data to support urban design. The results show that the method can effectively formulate urban design decisions. All these studies have achieved certain results, and the generated models reflect consideration of the surrounding urban fabric, indicating the feasibility of smart city site selection through artificial intelligence technology.

3. Methodology

3.1. Improved GAN Model Design Based on Multimedia Data. The GAN consists of two parts, namely, a generator and a discriminator. The generator generates new samples by learning the probability distribution of real multimedia data. The discriminator determines whether the input data are real multimedia data, and both improve the quality of the generated samples through game learning. CGAN is a generative network that improves on GAN. It combines supervised and unsupervised learning and adds label information to the input of the model, which can be used to guide the generation of multimedia data. CGAN is a method to implicitly learn the probability distribution of historical multimedia data from it using game adversarial ideas, as shown in Figure 1. By training the generator and discriminator alternately, the final effect is to transform the noise into a probability distribution similar to the historical data. CGAN can map the noise into different conditional probability distributions according to the given different conditional information and has good generation ability for multimedia data from multiple distributions.

As can be seen from Figure 1, the conditional information c and the noise vector k are used as the inputs of the generator A. The generator A outputs the generated samples $i' = A(k|c)$. The discriminator D determines whether the generated sample i' satisfies the conditional information c while judging the similarity between the generated sample distribution $u(i')$ and the real sample distribution $u(i)$. The loss functions of the generator and discriminator in CGAN are shown in the following:

Table 2: Partial GAN network development genealogy.

Classification by conditional information	Classification by model structure	Classification by loss function	Classification image by transformation
CGAN	DCGAN	LSGAN	Pix2pix
ACGAN	LAPGAN	WGAN	Pix2pixHD
TripleGAN	StackGAN	WGAN-GP	FUNIT
—	—	—	—

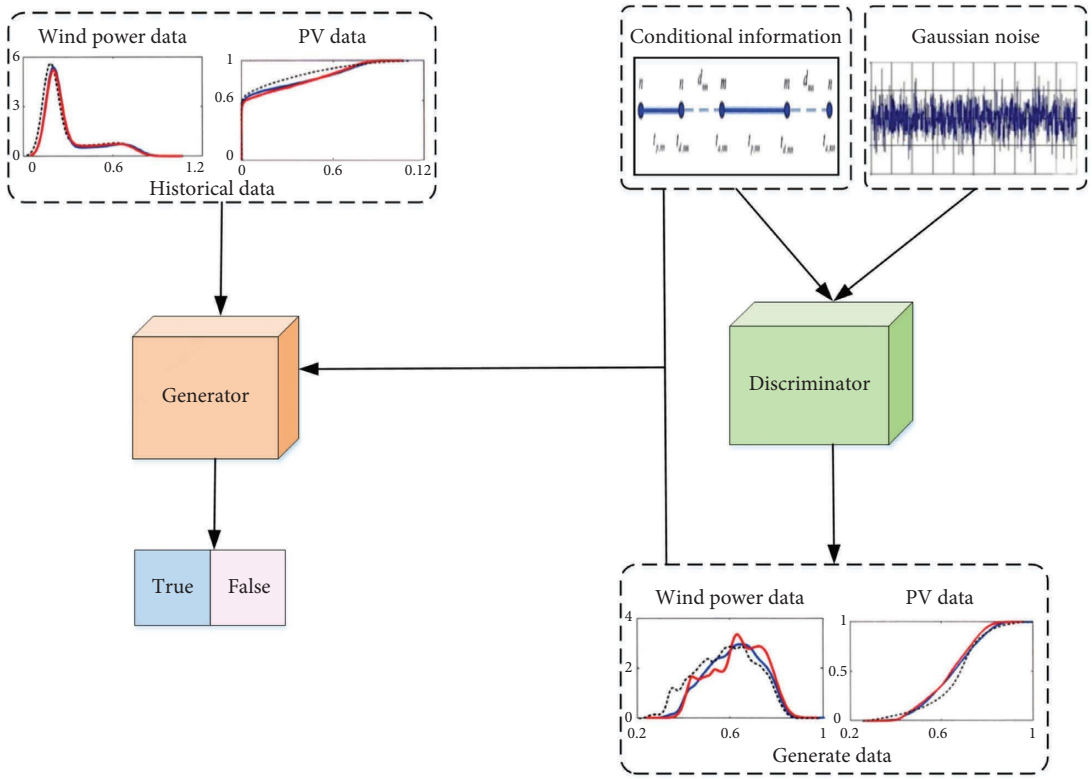

Figure 1: Basic structure of CGAN based on multimedia data.

$$\text{Loss}_A = -E_{i' \sim u(i')}\left[D\left(i'|c\right)\right], \tag{1}$$

$$\text{Loss}_D = -E_{i \sim u(i)}\left[D\left(i|c\right)\right] + E_{i' \sim u(i')}\left[D\left(i'|c\right)\right], \tag{2}$$

where E is the expected value of the corresponding distribution, $D(\sim)$ is the discriminator function, c represents conditional information, z represents noise vectors, A represents the generator, and D represents the discriminator. The loss function of the generator (Loss_A) is optimized by maximizing the probability of the discriminator, classifying the generated samples as real. The generator aims to deceive the discriminator by generating samples that cannot be accurately distinguished as fake. Therefore, the generator's objective is to minimize the negative logarithm of the discriminator's probability of classifying the generated samples as real. The loss function of the discriminator (Loss_D) is optimized by maximizing its ability to accurately distinguish between generated samples and real samples. The discriminator aims to correctly classify both types of samples. Thus, the discriminator's objective is to maximize the sum of two probabilities, i.e., the negative logarithm of the discriminator's probability of classifying real samples as real and the negative logarithm of the discriminator's probability of classifying generated samples as fake. The generator aims to minimize its loss function (Loss_A), while the discriminator aims to minimize its loss function (Loss_D). Through alternating training of the generator and discriminator and continuously optimizing them, the generator can generate realistic samples that match the given condition, and the discriminator can accurately differentiate between generated and real samples. Eventually, the generator and discriminator gradually reach a balance during the training process, resulting in high-quality generated samples.

In the process of CGAN training, the training objective is the minimal-maximal game with conditions, as shown in the following equation:.

$$\min_{A} \max_{D} Q(A, D) = E_{i\sim u(i)}[D(i|c)] - E_{i'\sim u(i')}\left[D\left(i'|c\right)\right]. \tag{3}$$

At the end of training, the generator A can learn the probability distribution characteristics of the real sample i and thus can generate multimedia data obeying the real law under the conditional information c.

The traditional GAN often encounters training difficulties and suffers from pattern collapse, leading to a decrease in the accuracy of generated samples i'. To address these issues, the loss function based on the Wasserstein distance is adopted as a replacement for the JS divergence used in the traditional GAN [23]. The Wasserstein distance is capable of quantifying the similarities between two distinct probability distributions, where a smaller value indicates a higher degree of similarity. It is defined as shown in the following equation:.

$$M\left(u(i), u\left(i'\right)\right) = \inf_{\pi(i,i')} \int d\left(i, i'\right)\pi\left(\mathrm{d}i, \mathrm{d}i'\right), \tag{4}$$

where $\pi(i, i')$ is the joint probability density distribution, satisfying the marginal distributions of $u(i)$ and $u(i')$, $d(i, i')$ is the interscenario distance measure, and "inf" indicates the lower bound (infimum), which is the maximum lower bound. The Wasserstein distance is generally solved in the Kantorovich–Rubinstein dual form, which is applied to WGAN, as shown in the following equation:

$$M_{\left(u_i, u_{i'}\right)} = \sup_{\|f_D\|_L \leq 1} E_{u(i)}[D(i|c)] - E_{u(i')}\left[D\left(i'|c\right)\right], \tag{5}$$

where $\|f_D\|_L \leqslant 1$ means that the discriminator D needs to satisfy the 1-Lipschitz continuum. In this paper, the loss function of discriminator D is modified by adding a gradient penalty term to the original loss function to make it satisfy the 1-Lipschitz condition restriction. The specific form is shown inthe following equation:

$$AU|_{\widehat{i}} = \lambda E_{\widehat{i}\sim u(\widehat{i})}\left[\left(\left\|\nabla_{\widehat{i}} D(\widehat{i})\right\|_u - 1\right)^2\right], \tag{6}$$

where $\|.\|_u$ denotes the u parameter; λ denotes the regular term coefficient; $\widehat{i}$ is obtained by random interpolation sampling on the line between the real sample i and the generated sample i'. $\widehat{i} = \varepsilon i + (1 - \varepsilon)i'$ and ε obey a uniform distribution on [0, 1]. In summary, the overall training objective function of WGAN-GP is as follows:

$$\min_{A} \max_{D} Q(A, D) = E_{i\sim u(i)}[D(i|c)] - E_{i'\sim u(i')}\left[D\left(i'|c\right)\right] - \lambda E_{\widehat{i}\sim u(\widehat{i})}\left[\left(\left\|\nabla_{\widehat{i}} D(\widehat{i}|c)\right\|_u - 1\right)^2\right]. \tag{7}$$

A convolutional neural network is used instead of the traditional multilayer perceptron to construct the generator and discriminator, and the generator and discriminator are symmetric network structures. The generator has 4 layers, and the number of filters is 256, 128, 64, and 1. The size of the convolutional kernel is 5 in the first layer and 4 in the last 3 layers. The first 3 layers use ReLU [30] as the activation function, and the last layer uses Tanh as the activation function. A batch normalization (BN) layer is added after the first three convolutional layers to improve the robustness of the network. Considering that the BN layer will be the output normalized to a normal distribution of $N(0, 1)$, the BN layer is not added after the output layer. The discriminator is also 4-layer, the convolution kernel size is 4, and the number of filters is 16, 32, 64, and 1. The first 3 layers use Leaky ReLU [31] as the activation function. Due to the structural characteristics of the WGAN-GP model, no activation function is added to the last layer. The network structures and parameters of the generator and discriminator are shown in Figures 2 and 3, respectively.

Due to the variation in wind power and solar power output with seasons and weather conditions, they exhibit strong randomness and volatility. Therefore, relying solely on the daily values of multimedia data as planning parameters would lead to unreasonable results in distributed power generation planning. This paper is based on the concept of a multimedia dataset and wind-solar power output scenarios. It utilizes the WGAN-GP model to learn the distribution of historical wind-solar data and generates a collection of multimedia wind-solar power output scenarios that include multiple dimensions such as wind speed, solar radiation, air humidity, cloud coverage, temperature, and rainfall. These multiple dimensions of data provide more comprehensive environmental characteristics to accurately describe the wind-solar power output scenarios. These scenario collections comprehensively consider the predictive capabilities of wind power and solar power systems at different times and locations, incorporating multimedia information. However, conducting extensive simulation calculations based on the entire dataset is challenging due to the enormous computational load. To address this issue while considering the temporal and stochastic nature of wind-solar power output, this paper applies the K-means clustering algorithm to analyze and cluster the generated multimedia wind-solar power output scenarios. The clustering categorizes the multimedia wind-solar power output scenarios under different seasons and weather conditions into typical categories such as sunny, cloudy, and rainy, resulting in twelve clustered scenarios. These multimedia wind-solar power output scenarios provide

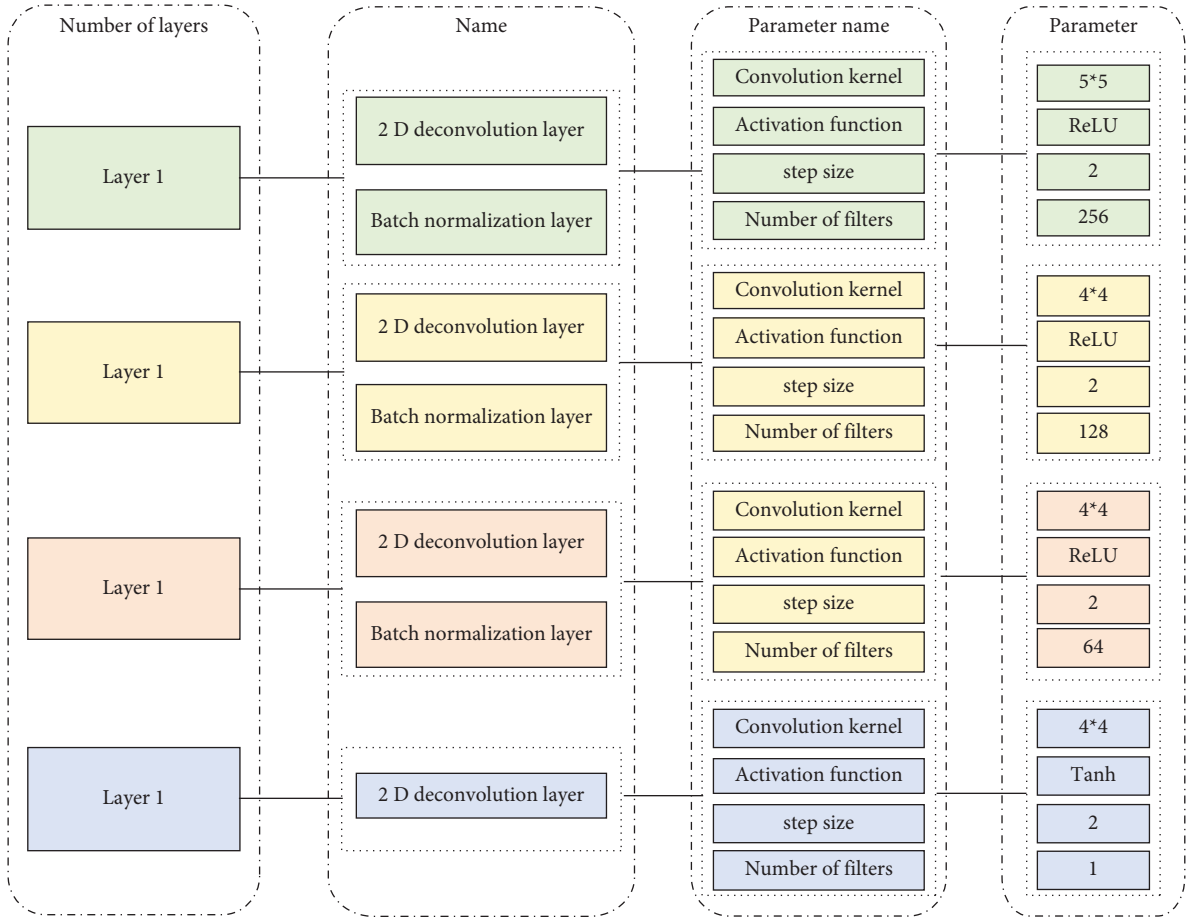

Figure 2: Generator structure diagram.

a comprehensive description of the output capabilities of wind power and solar power systems by integrating multiple dimensions of data, including wind speed, solar radiation, temperature, and humidity. These scenarios reflect the variations in energy production under different environmental conditions. Generating and analyzing multimedia wind-solar power output scenarios through clustering contributes to the decision-making process in energy planning, system design, and operational management.

The specific steps of K-means clustering are as follows:

(1) According to the four seasons of the year, the scenery output scenarios under different seasons are clustered into three typical scenarios, namely, sunny, cloudy, and rainy, so there are 12 scenarios after clustering.

(2) 12 scenarios are randomly selected from the original output scenario set as the initial clustering center $N^{(0)} = (\psi_1^{(0)}, \psi_2^{(0)}, \cdots\cdots \psi_z^{(0)})$, $z = 12$.

(3) The Euclidean distance from each scenario to the cluster center is calculated separately, and each scenario is divided into the clusters with the closest distance. The formula for calculating the Euclidean distance from each scenario to the cluster center is as follows:

$$D(\psi_x, \psi_y) = \sqrt{\sum_{z=1}^{t} \left(\psi_x(z) - \psi_y(z)\right)^2}, \tag{8}$$

where $D(\psi_x, y)$ is the distance between scenario curves and $\psi_x(z)$ is the z-th dimensional data of the ith scenario.

(4) Calculate the centroids of each of the Z clusters and update the cluster centers $N^{(1)} = (\psi_1^{(1)}, \psi_2^{(1)}, \cdots\cdots, \psi_z^{(1)})$.

(5) Repeat steps (3) and (4), the final clustering center curve that corresponds to Z typical scenarios $\{\xi_1, \xi_2, \cdots\cdots, \xi_z\}$.

The K-means clustering algorithm plays a key role in our site-selection recommendation algorithm. By clustering the dataset, we were able to identify representative site-selection scenarios and capture the relationship between multimedia data and optimal facility locations. Clustering facilitates generalization to unseen scenarios and improves the accuracy of our site selection recommendations. We then utilized these clusters in the recommendation process, training on the labeled datasets within each cluster. This training allowed the algorithm to learn the link between the city multimedia data and the best site selection decision. As a result, the

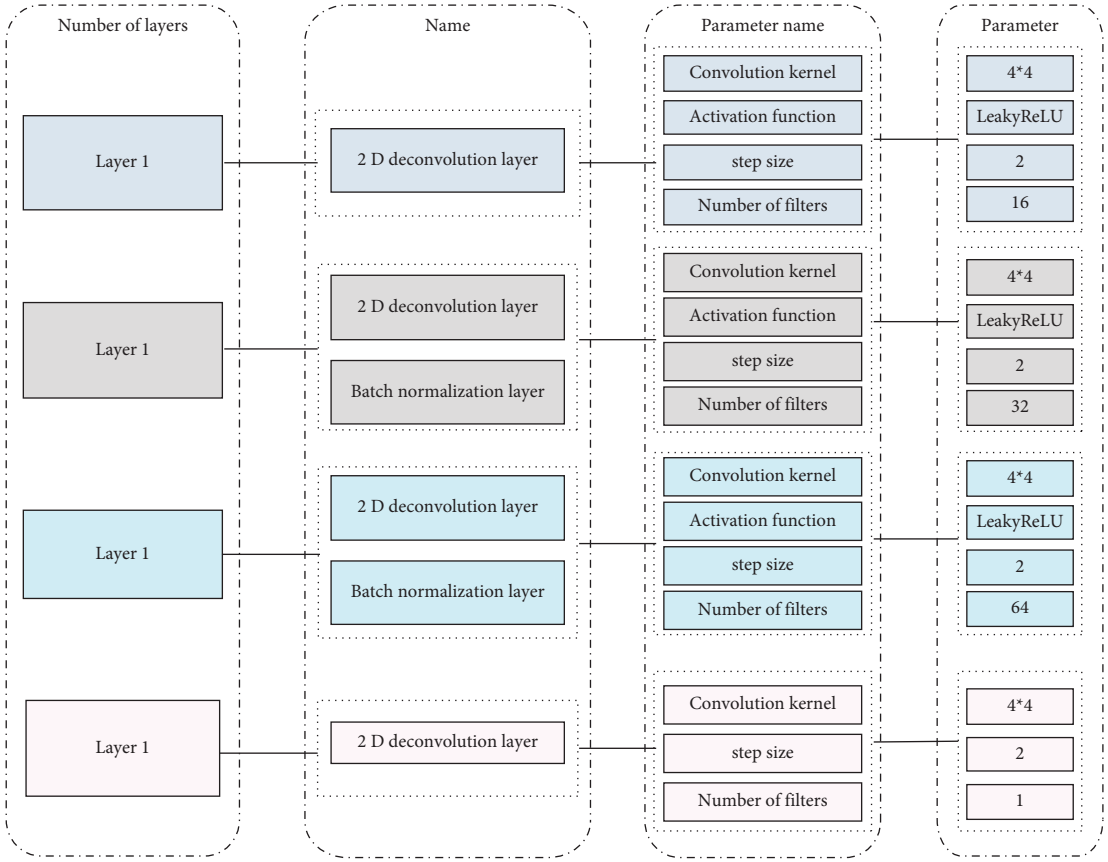

Figure 3: Discriminator structure diagram.

algorithm can use the knowledge gained from the clusters to provide informed and accurate recommendations when new scenarios are encountered.

3.2. DG Site Selection Model

3.2.1. Objective Function. In this paper, we study three DGs, namely, wind turbine (WT), photovoltaic (PV), and microturbine (MT), and develop an optimal allocation model for DGs with minimum annual integrated costs. The cost includes the construction investment cost, operation and maintenance cost, network loss cost, main grid purchase cost, and the environmental benefits generated by DG generation.

$$\min C = C_X + C_{OW} + C_L + C_U - C_S. \tag{9}$$

The mathematical expressions of the various costs of DG in (9) are as follows:

(1) Converting to the annual DG construction investment cost C_X, the value of which can be calculated by the following mathematical equation.

$$C_X = G(d, j) \sum_{z=1}^{T_{\text{type}}} \sum_{y \in \Omega^{DAz}} \left(c_X^{DAz} U_{r,y}^{DAz} \right), \tag{10}$$

where $G(d, j) = d(1 + d)^j / ((1 + d)^j - 1)$ denotes the present value to equal the annual value coefficient of DG. Here, d is the discount rate and j is the planning year. N_{type} is the type of DG, with 1 and 2 representing WT and PV, respectively, and y is the node where DG is installed. Ω^{DAz} is the set of nodes where the z-th type of DG is installed, c_I^{DAz} is the construction investment cost coefficient per unit capacity of the z-th type of DG installed at node y, and $U_{r,y}^{\text{DAz}}$ is the rated capacity of the z-th type of DG installed at node y.

(2) DG annual operation and maintenance costs, C_{OW}:

$$C_{OW} = n_d \omega_s \sum_{s=1}^{T_s} \sum_{n \in N} \sum_{z=1}^{T_{\text{type}}} \sum_{y \in \Omega^{\text{DAz}}} c_{OW}^{\text{DAz}} U_{y,s,n}^{\text{DAz}}, \tag{11}$$

where $n_d = 365$; ω_s is the probability of occurrence of scenario s; T_s is the total number of scenarios; c_{OW}^{DAz} is the operation and maintenance cost factor required for the z-th DG installed at node y to emit a unit of power; and $U_{y,s,n}^{\text{DAz}}$ is the active power emitted by the z-th DG installed at node y at moment t of scenario s.

(3) Network loss cost, C_L

$$C_L = n_d \omega_s \sum_{s=1}^{T_s} \sum_{n \in N} \sum_{xy \in \Omega^{\text{Grid}}} \left(c_{\text{Loss}} X_{xy,s,n}^2 r_{xy} \right), \tag{12}$$

where Ω^{Grid} is the set of all nodes; c_{Loss} is the network loss cost factor; $I_{xy,s,n}$ denotes the current flowing

from node x to node y at moment n for scenario s; and r_{xy} denotes the resistance value of the line between node x and node y.

(4) The value of C_u: the cost of purchasing power from the upper grid can be calculated by the following mathematical equation:

$$C_U = n_d \omega_s \sum_{s=1}^{Ts} \sum_{n \in N} \sum_{y \in \Omega^{NR}} \left(c_{NR} U_{y,s,n}^{NR} \right), \tag{13}$$

where Ω^{NR} is the set of transformer nodes; c_{NR} is the unit power purchase cost coefficient of power purchased from the main grid; and $U_{y,s,n}^{NR}$ is the amount of power purchased from the main grid.

(5) Environmental benefits of DG generation, C_s: environmental benefits include 2 components, namely, environmental pollution costs and government subsidies. Here, the environmental pollution cost is the compensation cost of environmental pollution generated by MT power generation. Government subsidies are the benefits generated by DG generation.

$$C_S = n_d \omega_s \left(\sum_{s=1}^{T_s} \sum_{n \in N} \left(\sum_{y \in \Omega^{MT}} \sum_{m=1}^{t} (Q_m + F_m) D_m U_{y,s,n}^{MT} - \sum_{z=1}^{T_{\text{type}}} \left(c_f U_{y,s,n}^{\text{DAz}} \right) \right) \right), \tag{14}$$

where Ω^{MT} is the set of nodes where MTs are installed. V_m and F_m are the environmental values of the pollutant and the penalty imposed, respectively. D_m is the emission of the pollutant. $U_{y,s,n}^{MT}$ is the active power emitted by the MT installed at node y at time n under scenario s. c_f is the government subsidy cost factor.

3.2.2. Constraint Conditions. In the planning process, we consider the tidal current constraint, nodal voltage constraint, branch current constraint, transformer power saving constraint, and DG-related constraints, as described.

(1) Power flow constraint [32]:

$$\begin{aligned}
\sum_{z \in \delta(y)} U_{yz,s,n} - \sum_{x \in \pi(y)} \left(U_{xy,s,n} - X_{xy,s,n}^2 r_{xy} \right) &= \sum_{y \in \Omega^{NR}} U_{y,s,n}^{NR} + \sum_{z=1}^{T_{\text{type}}} \sum_{y \in \Omega^{\text{DAz}}} U_{y,s,n}^{\text{DAz}} - \sum_{y \in \Omega^{\text{Grid}}} U_{y,s,n}^{\text{Load}}, \\
\sum_{z \in \delta(y)} V_{yz,s,n} - \sum_{x \in \pi(y)} \left(V_{xy,s,n} - X_{xy,s,n}^2 i_{xy} \right) &= \sum_{y \in \Omega^{NR}} V_{y,s,n}^{NR} + \sum_{z=1}^{T_{\text{type}}} \sum_{y \in \Omega^{\text{DAz}}} V_{y,s,n}^{\text{DAz}} - \sum_{y \in \Omega^{\text{Load}}} V_{y,s,n}^{\text{Load}}, \\
P_{y,s,n}^2 &= P_{x,s,n}^2 - 2\left(U_{xy,s,n} r_{xy} + V_{xy,s,n} i_{xy} \right) + X_{xy,s,n}^2 \left(r_{xy}^2 + i_{xy}^2 \right), \\
X_{xy,s,n}^2 &= \frac{U_{xy,s,n}^2 + V_{xy,s,n}^2}{P_{y,s,n}^2},
\end{aligned} \tag{15}$$

where $\delta(y)$ is the set of endpoints; $\pi(y)$ is the set of starting points; $U_{xy,s,n}$ and $V_{xy,s,n}$ denote the active and reactive power flowing from node x to node y in time period n for scenario s, respectively. r_{xy} and i_{xy} denote the resistance and reactance values of the line between node x and node y. $V_{y,s,n}^{NR}$ and $V_{y,s,n}^{D,z}$ are the reactive power of the transformer and the z-th DG connected to node y at time period n of the s scenario, respectively. $U_{y,s,n}^{\text{Load}}$ and $V_{y,s,n}^{\text{Load}}$ are the reactive power of the transformer and the z-th DG connected to node y at time period n of the s scenario, respectively. $P_{y,s,n}$ and $P_{x,s,n}$ are the voltage amplitudes of node y and node x in the time period n of scenario s, respectively.

(2) Node voltage constraint:

$$U_{\min} \leqslant U_{y,s,n} \leqslant U_{\max}, \tag{16}$$

where $P_{\max}$ and $U_{\min}$ are the upper and lower limits of the voltage at node y, respectively.

(3) Branch current constraint [33]:

$$0 \leqslant I_{xy,s,n} \leqslant I_{\max}, \tag{17}$$

where $I_{\max}$ is the maximum value of current allowed in branch y.

(4) Transformer power saving power constraint:

$$\begin{cases} U_y^{NR,\min} \leqslant U_{y,s,n}^{NR} \leqslant U_y^{NR,\max}, \\ V_y^{NR,\min} \leqslant V_{y,s,n}^{NR} \leqslant V_y^{NR,\max}, \end{cases} \tag{18}$$

where $U_y^{NR,\max}$ and $U_y^{NR,\min}$ are the upper and lower limits of transformer active power, respectively. $V_y^{NR,\max}$ and $V_y^{NR,\min}$ are the upper and lower limits of transformer reactive power, respectively.

(5) DG-related constraints:

$$\begin{cases} 0 \leqslant U_{y,s,n}^{\mathrm{DAz}} \leqslant U_{y,s,n}^{\mathrm{DAz,max}}, \\ 0 \leqslant V_{y,s,n}^{\mathrm{DAz}} \leqslant V_{y,s,n}^{\mathrm{DAz,max}}, \\ 0 \leqslant U_{r,y}^{\mathrm{DAz}} \leqslant U_{r,y}^{\mathrm{DAz,max}}, \\ \sum_{z=1}^{T_{type}} \sum_{y \in \Omega^{\mathrm{DAz}}} U_{r,y}^{DAz} \leqslant \mu U_{L\mathrm{total}}, \end{cases} \tag{19}$$

where $U_{y,s,n}^{\mathrm{DAz,max}}$ is the upper limit of the active power output of DG installed at node y. $V_{y,s,n}^{\mathrm{DAz,max}}$ is the upper limit of the reactive power output of DG installed at node y. $U_{r,y}^{\mathrm{DAz,max}}$ is the maximum capacity of DG allowed to be installed at node y; μ is the penetration rate. $U_{L\mathrm{total}}$ is the total active load of the distribution network. Finally, the process of solving the DG optimal planning model using the commercial software CPLEX is shown in Figure 4. Here, the *K*-means clustering method to eliminate the situation can be referred to in several steps before and after equation (8).

4. Result Analysis and Discussion

4.1. Scenario Setting. In order to verify the advantages and solution results of the model proposed in this paper, two scenarios are designed for analysis and comparison with different factors affecting DG. Scenario 1: DG is installed under the planning scenario proposed in this paper, and scenario 2: DG is installed under the wind power output only, without considering PV.

The data used in this paper are collected and obtained from multiple sources, respectively, by the following methods:

(1) Electric vehicle charging piles: we collaborate with electric vehicle charging infrastructure providers to access data on charging behaviors and usage patterns.

(2) Power distribution: we collaborate with power distribution companies to obtain historical data on network operations and load demand.

(3) Wind power and photovoltaic generation: we collaborate with renewable energy companies to obtain historical generation data from wind farms and solar installations.

(4) IoT: we collaborate with IoT platform companies that specialize in IoT solutions to access aggregated or real-time IoT data.

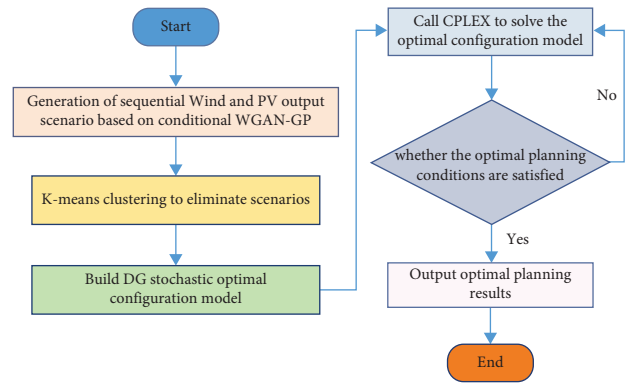

Figure 4: Flow chart of DG planning based on WGAN-GP.

4.2. Scenario Comparison Analysis. The models in scenario 1 and scenario 2 are solved separately, and the results are compared and analyzed. The comparison of the costs under scenario 1 and scenario 2 is shown in Figure 5.

According to Figure 5, compared with the planning cost, scenario 1 is much lower than scenario 2. The reason is that Scenario 1 can save part of the planning cost by making a reasonable planning of charging stations with the model in this paper. Comparing the network loss cost, it shows that scenario 1 is more advantageous. This is due to the reasonable allocation of DG in the distribution network, which reduces the power flow constraint in the distribution network and effectively reduces the network loss. Comparing the operation costs, scenario 1 is higher than scenario 2. It indicates that scenario 2 does not consider that the PV output will increase the voltage difference between the first and the end of the line, thus affecting the benefit of the distribution system when it actually operates. Comparing the total cost, scenario 1 saves 21.95% of the total cost compared to scenario 2. The service life of charging stations is typically 15–20 years, making scenario 1 more advantageous from a long-term development perspective.

With the increased construction and use of DG, the total amount of EV charging load and conventional load will also grow year by year, which will greatly affect the branch currents in the distribution network and lead to the branch currents crossing the limit under bad conditions, affecting the stable operation of the charging piles of the system. As shown in Figure 6, the number of overrunning branch circuits in different scenarios.

It is clear from Figure 6 that when the total load increases by 44%, the lines that cross the limit appear in scenario 2. When the total load increases by 50%, the number of lines that cross the limit increases to 3. When the total load increases by 56%, the out-of-bounds lines start to appear in scenario 1. When the load increases further, the number of out-of-limit lines in scenario 1 increases to 2. Through comparative analysis, scenario 1 can significantly withstand the growth of total load by reasonably matching the location of the DG and charging station and effectively improving the situation of branch circuit current overruns, thus improving the stable operation of the distribution network.

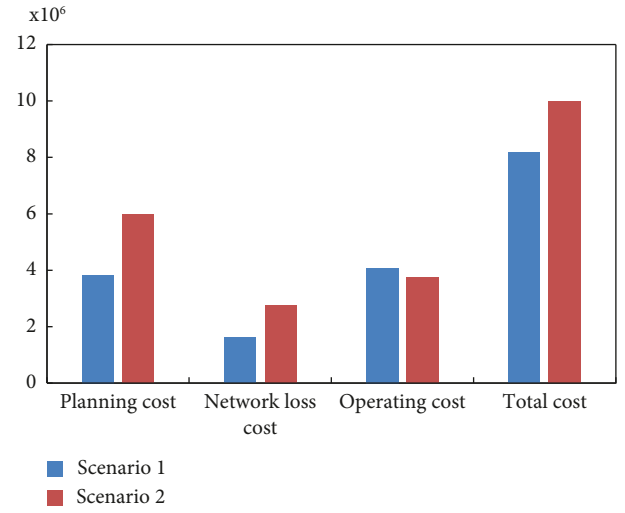

Figure 5: Comparison of various costs under scenario 1 and scenario 2.

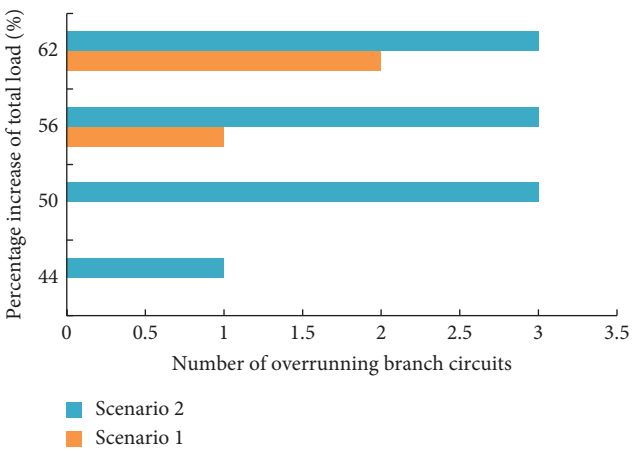

Figure 6: Number of branch current crossing in 2 scenarios.

In this section, we take a region 2021 EV charging station, user demand point, and DG collaborative planning as examples and establish an *xy* coordinate system to get the coordinates of DG candidate points under 2 scenarios. The topology of the DG planning connections corresponding to the coordinates *x*, *y* under scenario 1 and scenario 2 are shown in Figures 7 and 8.

It can be seen from the above figures that the distribution of DG candidate points in scenario 1 is relatively average, which can meet the charging demand of more EV users. Considering the local consumption of DG by EV charging stations, the DG candidate sites in scenario 1 are selected near EV charging stations and user demand points. This realizes the local consumption of DG with high penetration rate and reduces the pressure of EV load on the distribution network. In scenario 2, DG candidates are unevenly distributed, and many customer demand points are far away from DG candidates.

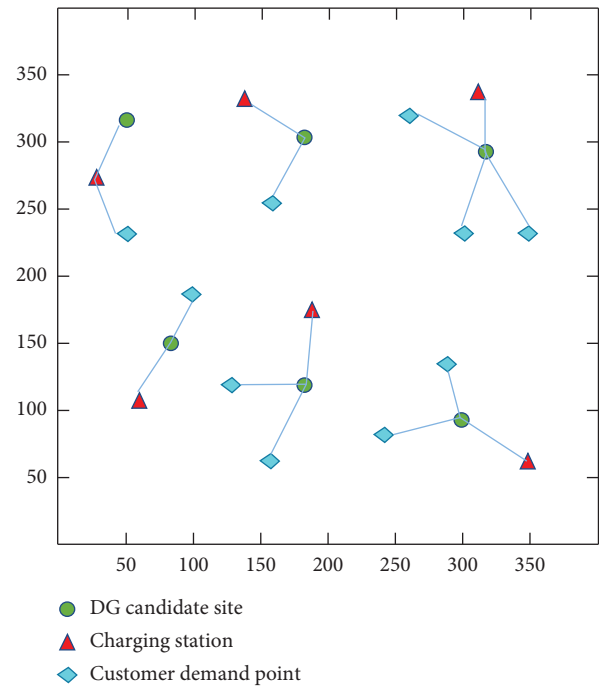

Figure 7: Schematic diagram of DG planning connection topology under scenario 1.

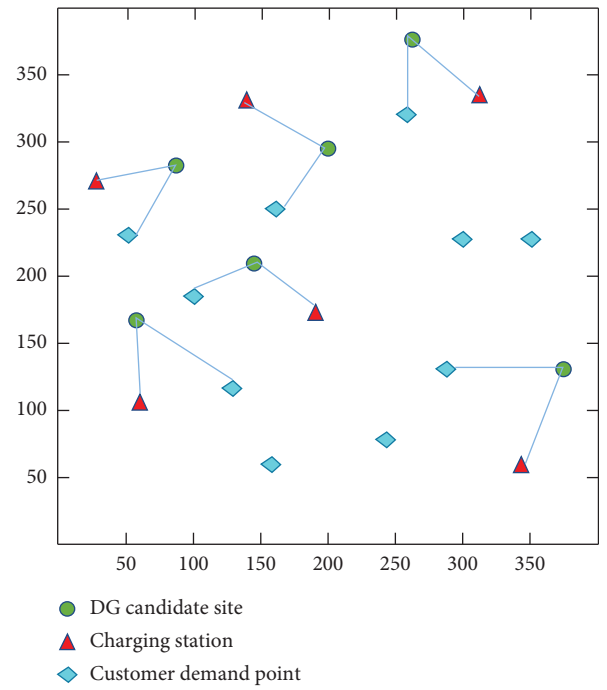

Figure 8: Schematic diagram of DG planning connection topology under scenario 2.

4.3. Comparison of Algorithm Efficiency. In order to further verify the rapidity and accuracy of the algorithm in this paper, the algorithms of literature [34], literature [35], and the proposed algorithm were used simultaneously to carry out the optimization search. The three optimization algorithms were used to plan the optimization search under

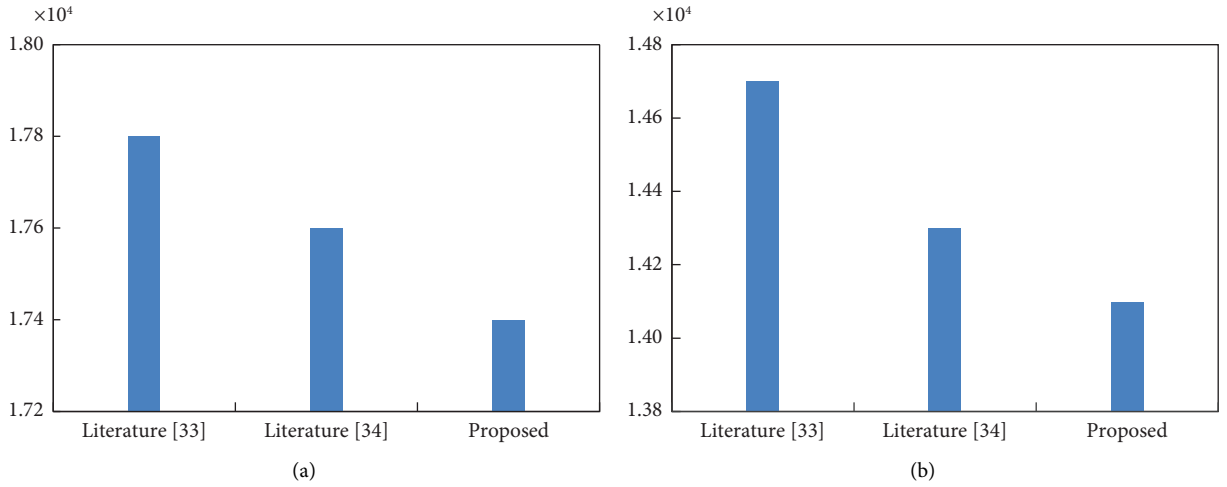

Figure 9: Comparison of adaptation values. (a) Scenario 1. (b) Scenario 2.

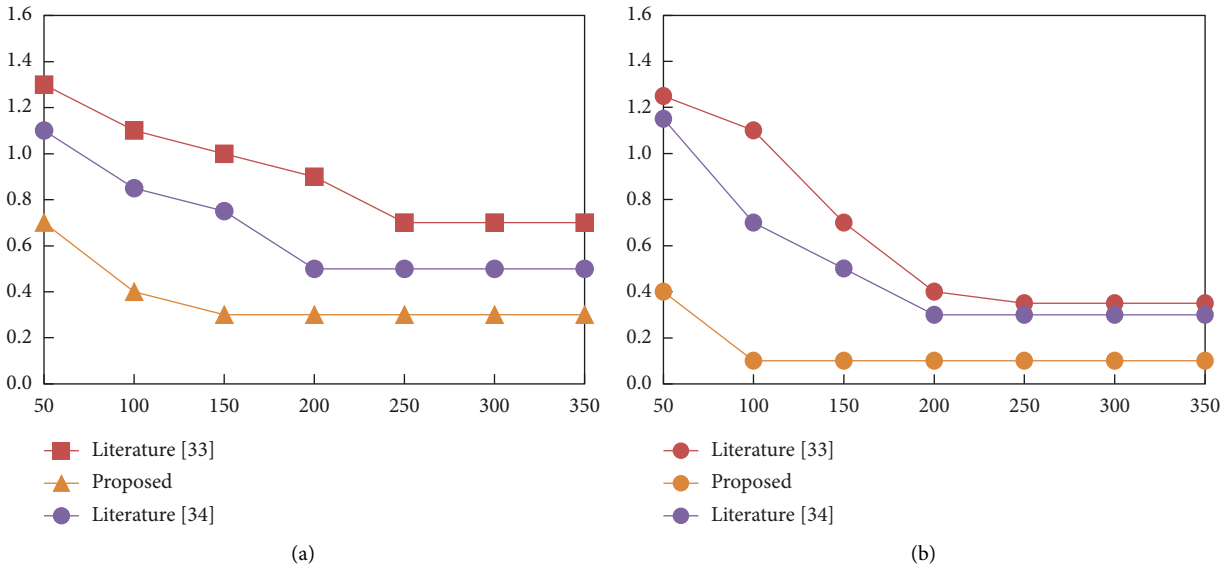

Figure 10: Convergence performance comparison. (a) Scenario 1. (b) Scenario 2.

scenario 1 and scenario 2, respectively, and repeated 40 times, and the adaptation values of each optimization algorithm in scenario 1 and scenario 2 were obtained as shown in Figure 9. The analysis of Figure 9 shows that in the repeated experiments of scenario 1 and scenario 2, the upper and lower ranges and median values of the fitness function obtained by the algorithms in this paper are the smallest compared with those in literature [34] and literature [35], which prove that this paper is more effective in the process of seeking the best.

Figure 10 shows the comparison of the convergence speed of the three algorithms in literature [34], literature [35], and the algorithm in this paper for scenario 1 and scenario 2.

The comparison of the legend clearly shows that the algorithm in this paper has the least number of iterations and the fastest speed among the three algorithms. Also, comparing the final convergence values of the three algorithms, it is obvious that the results of the proposed algorithm are more economical. Therefore, this algorithm works better at solving DG planning and EV charging problems.

5. Conclusion

In today's world, the increasing scarcity of traditional energy sources and the pressing issue of environmental pollution have led to the widespread adoption of distributed generations (DGs) and electric vehicles (EVs) as effective solutions to address the energy crisis and pollution problems. Planning DGs in a rational manner to meet the growing demand for the distribution load and traffic load has become a crucial task to be addressed. This paper takes into account the multimedia data characteristics of wind and photovoltaic (PV) output scenarios and proposes the use of the

WGAN-GP model to generate multimedia data for these scenarios. By doing so, it overcomes the problem of generating unreasonable scenarios that arise from the disparities between the assumed and real data distributions in traditional sampling methods. The generated scenarios are further reduced using the *K*-means clustering algorithm, which simplifies the complexity of modeling and calculation. Moreover, an optimal planning model is formulated with the objective of minimizing the annual comprehensive cost. Comparative analysis with other planning schemes demonstrates that the proposed scheme in this paper is not only the least costly but also more reasonable, thus contributing to the advancement and development of DG in the future. The approach presented in this paper not only provides multimedia data support for DG planning but also lays the foundation for subsequent analysis of EV charging load spatiotemporal distribution and the planning of EV charging stations. In future work, it is recommended to consider other types of DGs to further enhance the reliability of distribution networks and improve the integration of energy storage devices for EV charging stations.

Data Availability

The labeled datasets used to support the findings of this study are available from the corresponding author upon request.

Conflicts of Interest

The authors declare that there are no conflicts of interest.

Authors' Contributions

Ming He contributed to the writing of the manuscript and data analysis. Xueqing Xie made important contributions to the revision, provided great help in the revision of the final draft, and agreed to be included in the authors' list of the article. All the authors unanimously agreed to the above arrangement. All the authors have read and agreed the final version to be published.

Acknowledgments

This work was supported in part by the the Chongqing Social Science Planning Project, "Research on Sustainable Development and application of digital resources of Bashu witch culture" (No. 2020YBYS192).

References

[1] W. Qi and Z. J. M. Shen, "A smart-city scope of operations management," *Production and Operations Management*, vol. 28, no. 2, pp. 393–406, 2019.

[2] A. Chamra and H. Harmanani, "A smart greenhouse control and management system using IoT," in *Proceedings of the 17th International Conference on Information Technology–New Generations (ITNG 2020)*, pp. 641–646, Springer International Publishing, Tuscany Suites, LV, USA, April 2020.

[3] M. Adhikari, L. P. Ghimire, Y. Kim, P. Aryal, and S. B. Khadka, "Identification and analysis of barriers against electric vehicle use," *Sustainability*, vol. 12, no. 12, p. 4850, 2020.

[4] C. T. Ma, "System planning of grid-connected electric vehicle charging stations and key technologies: a review," *Energies*, vol. 12, no. 21, p. 4201, 2019.

[5] R. A. Ufa, Y. Y. Malkova, V. E. Rudnik, M. V. Andreev, and V. A. Borisov, "A review on distributed generation impacts on electric power system," *International Journal of Hydrogen Energy*, vol. 47, no. 47, pp. 20347–20361, 2022.

[6] L. Liu, F. Xie, Z. Huang, and M. Wang, "Multi-objective coordinated optimal allocation of DG and EVCSs based on the V2G mode," *Processes*, vol. 9, no. 1, p. 18, 2020.

[7] A. G. Veeresha, H. M. Prasanna, M. L. Kumar, and T. Ananthapadmanabha, "An adaptive power system management with DG placement and cluster-based load forecasting by CS, K-means and ANN algorithms," *International Journal of Power Electronics*, vol. 13, no. 3, pp. 380–398, 2021.

[8] S. He, H. Gao, H. Tian, L. Wang, Y. Liu, and J. Liu, "A two-stage robust optimal allocation model of distributed generation considering capacity curve and real-time price-based demand response," *Journal of Modern Power Systems and Clean Energy*, vol. 9, no. 1, pp. 114–127, 2021.

[9] S. Jiménez-Fernández, C. Camacho-Gómez, R. Mallol-Poyato et al., "Optimal microgrid topology design and siting of distributed generation sources using a multi-objective substrate layer Coral Reefs Optimization algorithm," *Sustainability*, vol. 11, no. 1, p. 169, 2018.

[10] C. Venkatesan, R. Kannadasan, M. H. Alsharif, M. K. Kim, and J. Nebhen, "A novel multiobjective hybrid technique for siting and sizing of distributed generation and capacitor banks in radial distribution systems," *Sustainability*, vol. 13, no. 6, p. 3308, 2021.

[11] S. Panda, S. Mohanty, P. K. Rout et al., "An insight into the integration of distributed energy resources and energy storage systems with smart distribution networks using demand-side management," *Applied Sciences*, vol. 12, no. 17, p. 8914, 2022.

[12] A. Shuaibu Hassan, Y. Sun, and Z. Wang, "Optimization techniques applied for optimal planning and integration of renewable energy sources based on distributed generation: recent trends," *Cogent Engineering*, vol. 7, no. 1, Article ID 1766394, 2020.

[13] J. Jallad, S. Mekhilef, H. Mokhlis, J. Laghari, and O. Badran, "Application of hybrid meta-heuristic techniques for optimal load shedding planning and operation in an islanded distribution network integrated with distributed generation," *Energies*, vol. 11, no. 5, p. 1134, 2018.

[14] C. D. Prakash and L. J. Karam, "It GAN DO better: GAN-based detection of objects on images with varying quality," *IEEE Transactions on Image Processing*, vol. 30, pp. 9220–9230, 2021.

[15] W. Qian, H. Li, and H. Mu, "Circular lbp prior-based enhanced GAN for image style transfer," *International Journal on Semantic Web and Information Systems*, vol. 18, no. 2, pp. 1–15, 2022.

[16] H. Zhang, V. Sindagi, and V. M. Patel, "Image de-raining using a conditional generative adversarial network," *IEEE Transactions on Circuits and Systems for Video Technology*, vol. 30, no. 11, pp. 3943–3956, 2020.

[17] B. Erol, S. Z. Gurbuz, and M. G. Amin, "Motion classification using kinematically sifted acgan-synthesized radar micro-Doppler signatures," *IEEE Transactions on Aerospace and Electronic Systems*, vol. 56, no. 4, pp. 3197–3213, 2020.

[18] A. R. Sajun and I. Zualkernan, "Survey on implementations of generative adversarial networks for semi-supervised learning," *Applied Sciences*, vol. 12, no. 3, p. 1718, 2022.

[19] W. S. Lai, J. B. Huang, N. Ahuja, and M. H. Yang, "Fast and accurate image super-resolution with deep laplacian pyramid networks," *IEEE Transactions on Pattern Analysis and Machine Intelligence*, vol. 41, no. 11, pp. 2599–2613, 2019.

[20] S. Sharma, V. Kumar, and S. S. Sharma, "SIMULATION and designing of THREE-STACK GaN hemt power amplifier for 2-6 GHz bandwidth," *Journal of Engineering Science & Technology*, vol. 17, no. 4, pp. 2525–2544, 2022.

[21] H. Chen, F. Chen, and H. He, "SSC-GAN: a novel GAN based on the same solution constraints of first-order ODEs," *International Journal of Pattern Recognition and Artificial Intelligence*, vol. 35, no. 11, Article ID 2152018, 2021.

[22] Y. Li, J. Li, and Y. Wang, "Privacy-preserving spatiotemporal scenario generation of renewable energies: a federated deep generative learning approach," *IEEE Transactions on Industrial Informatics*, vol. 18, no. 4, pp. 2310–2320, 2022.

[23] Q. Yang, P. Yan, Y. Zhang et al., "Low-dose CT image denoising using a generative adversarial network with Wasserstein distance and perceptual loss," *IEEE Transactions on Medical Imaging*, vol. 37, no. 6, pp. 1348–1357, 2018.

[24] D. Newton, "Generative deep learning in architectural design," *Technology| Architecture+ Design*, vol. 3, no. 2, pp. 176–189, 2019.

[25] H. Zhao, M. Zhang, and F. Chen, "GAN-GL: generative adversarial networks for glacial lake mapping," *Remote Sensing*, vol. 13, no. 22, p. 4728, 2021.

[26] S. Ji, S. Wei, and M. Lu, "Fully convolutional networks for multisource building extraction from an open aerial and satellite imagery data set," *IEEE Transactions on Geoscience and Remote Sensing*, vol. 57, no. 1, pp. 574–586, 2019.

[27] K. Man and J. Chahl, "A review of synthetic image data and its use in computer vision," *Journal of Imaging*, vol. 8, no. 11, p. 310, 2022.

[28] Y. Li, Y. Ni, R. A. Croft, T. Di Matteo, S. Bird, and Y. Feng, "AI-assisted superresolution cosmological simulations," *Proceedings of the National Academy of Sciences of the United States of America*, vol. 118, no. 19, Article ID e2022038118, 2021.

[29] Y. Gong, P. Liao, X. Zhang et al., "Enlighten-GAN for super resolution reconstruction in mid-resolution remote sensing images," *Remote Sensing*, vol. 13, no. 6, p. 1104, 2021.

[30] J. A. Opschoor, P. C. Petersen, and C. Schwab, "Deep ReLU networks and high-order finite element methods," *Analysis and Applications*, vol. 18, no. 05, pp. 715–770, 2020.

[31] A. Maniatopoulos and N. Mitianoudis, "Learnable leaky relu (lelelu): an alternative accuracy-optimized activation function," *Information*, vol. 12, no. 12, p. 513, 2021.

[32] S. Karagiannopoulos, P. Aristidou, and G. Hug, "Data-driven local control design for active distribution grids using off-line optimal power flow and machine learning techniques," *IEEE Transactions on Smart Grid*, vol. 10, no. 6, pp. 6461–6471, 2019.

[33] J. Wang, N. Zhou, C. Y. Chung, and Q. Wang, "Coordinated planning of converter-based DG units and soft open points incorporating active management in unbalanced distribution networks," *IEEE Transactions on Sustainable Energy*, vol. 11, no. 3, pp. 2015–2027, 2020.

[34] W. Liu, F. Luo, Y. Liu, and W. Ding, "Optimal siting and sizing of distributed generation based on improved nondominated sorting genetic algorithm II," *Processes*, vol. 7, no. 12, p. 955, 2019.

[35] K. Balu and V. Mukherjee, "Optimal siting and sizing of distributed generation in radial distribution system using a novel student psychology-based optimization algorithm," *Neural Computing & Applications*, vol. 33, no. 22, pp. 15639–15667, 2021.